

Article

# Stepwise Construction of Ru(II) Center Containing Chiral Thiourea Ligand on Graphene Oxide: First Efficient, Reusable, and Stable Catalyst for Asymmetric Transfer Hydrogenation of Ketones

Gopiraman Mayakrishnan <sup>1</sup>, Kim Ick Soo <sup>2</sup> and Chung Ill Min <sup>1,\*</sup>

<sup>1</sup> Department of Crop Science, College of Sanghuh Life Science, Konkuk University, 120 Neungdong-ro, Gwangjin-gu, Seoul 05029, Korea; gopiramannitt@gmail.com

<sup>2</sup> Nano Fusion Technology Research Group, Division of Frontier Fibers, Institute for Fiber Engineering (IFES), Interdisciplinary Cluster for Cutting Edge Research (ICCER), Shinshu University, Tokida 3-15-1, Ueda 386-8567, Nagano Prefecture, Japan; kimicksoo.gr@gmail.com

\* Correspondence: imcim@konkuk.ac.kr; Tel.: +82-02-450-3730; Fax: +82-02-446-7856

Received: 1 November 2019; Accepted: 22 January 2020; Published: 2 February 2020



**Abstract:** Heterogenization of homogenous catalysts on solid support has attracted tremendous attention in organic synthesis due to the key benefits of heterogenized catalysts such as easy recovery and reusability. Although a considerable number of heterogenized catalysts are available, to the best of our knowledge, there is no efficient and reusable heterogenized catalyst reported for asymmetric reactions to date. Herein, we prepared a [RuCl<sub>2</sub>(η<sup>6</sup>-*p*-cymene)]/chiral thiourea ligand covalently bonded to graphene nanosheets (G-CLRu(II), where G represents graphene oxide (GO), CL denotes chiral *N*-((1-phenylethyl)carbamothioyl)acetamide and Ru(II) symbolizes [RuCl<sub>2</sub>(η<sup>6</sup>-*p*-cymene)]), for the asymmetric transfer hydrogenation of ketones. Five simple steps were involved in the preparation of the G-CLRu(II) catalyst. The structure of G-CLRu(II) was investigated by means of various spectroscopic and microscopic techniques. Coordination mode and covalent bonding involved in the G-CLRu(II) structure we reconfirmed. G-CLRu(II) demonstrated good catalytic performance towards the asymmetric transfer hydrogenation of ketones (conversion of up to 95%, enantiomeric excesses (ee) of up to 99%, and turnover number (TON) and turnover frequency (TOF) values of 535.9 and 22.3 h<sup>-1</sup>, respectively). A possible mechanism is proposed for the G-CLRu(II)-catalyzed asymmetric transfer hydrogenation of ketones. Recovery (~95%), reusability (fifth cycle, yield of 89% and ee of 81%), and stability of G-CLRu(II) were found to be good. We believe that the present stepwise preparation of G-CLRu(II) opens a new door for designing various metal-centered heterogenized chiral catalysts for asymmetric synthesis.

**Keywords:** graphene; chiral thiourea ligand; heterogenization; asymmetric reaction; reuse; recovery

## 1. Introduction

Catalytic asymmetric synthesis is a prime way to produce various pharmaceutically important chiral molecules [1,2]. Chiral alcohols obtained from the corresponding ketone via enantioselective synthesis are often found to play a significant role as intermediates in the synthesis of pharmaceuticals and agrochemicals [3]. Indeed, transition metal-catalyzed asymmetric transfer hydrogenation is a most suitable method to achieve such chiral alcohols in high yield with maximum enantiomeric excess [4]. To date, numerous transition metal complexes have been developed for homogeneous asymmetric catalysis [5–7]. Particularly, Ru(II)-chiral catalysts showed remarkable catalytic activity with high yield and selectivity. For instance, Baratta et al. [8], found cyclometalated Ru(II) complexes are highly

efficient for the asymmetric transfer hydrogenation of ketones using 2-propanol and NaOH. Similarly, Sheeba et al. [9] prepared chiral ( $\eta^6$ -*p*-cymene)–Ru(II) complexes containing acylthiourea ligands for the asymmetric transfer hydrogenation of ketones. In spite of the superior activity, the recovery and reusability of homogenous catalysts is highly limited. Heterogenization of homogenous catalysts on suitable solid support is found to be the most appropriate method to overcome the drawbacks [10]. A very small number of heterogenized catalysts have been developed for the asymmetric transfer hydrogenation of ketones. Among them, mesoporous silica nanosphere (MSN) is the most proffered platform for the immobilization of chiral–metal complexes. Mihalcik and Lin [11] used MSN as support for the heterogenization of chiral RuCl<sub>2</sub>–diphosphine–diamine complexes. The resultant heterogenized catalyst was found to be active and selective in the asymmetric hydrogenation of aromatic ketones. Sun et al. [12] introduced magnetically recoverable SiO<sub>2</sub>-coated Fe<sub>3</sub>O<sub>4</sub> nanoparticles as a new platform for anchoring a chiral Rh-catalyst. Similar to SiO<sub>2</sub>, other materials such as chitosan biopolymer [13], polyhedral oligomeric silsesquioxane [14], and Fe(0) nanoparticles [15] have also been employed. Recovery of these heterogenized catalysts is easily achieved; however, the reusability and enantioselectivity are often found to be moderate. Hence, developing a highly efficient, reusable, and selective heterogenized chiral catalyst for asymmetric hydrogenation is highly challenging and deserves special attention.

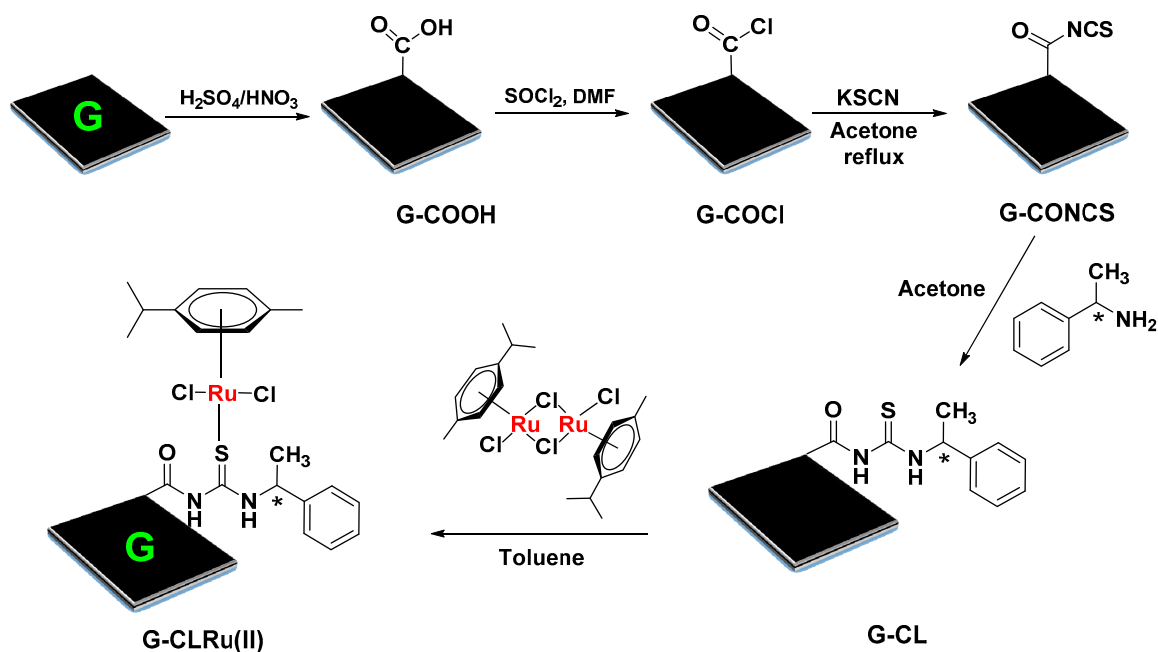
Graphene with a high surface area has played a substantial role in heterogeneous catalysis [16]. The heterogenization of active metal complexes on a graphene support has shown more versatility in carrying out highly selective catalytic processes [17]. Garrido-Barros et al. [18] heterogenized Cu(II) molecular catalysts on graphene surfaces to achieve a water oxidation reaction. They concluded that the electronic  $\pi$ -delocalization in graphene could boost the catalytic activity of graphene-anchored complexes. Active metal complexes, such as dioxomolybdenum(VI) [19], Cu(II)-salen and Co(II)-salen complexes [20,21], and Co(II), Fe(III), or VO(II) Schiff base metal complexes [22], are heterogenized on graphene sheets. The heterogenized graphene catalysts demonstrated good activity in various oxidation, reduction, and coupling reactions [23]. Unfortunately, there is a limited number of reports dealing with the heterogenization of chiral–metal complexes on graphene sheet. In fact, surface modification of graphene is often limited due to its chemical inertness. In spite of that, a simple acid treatment can generate various oxygen functional groups (such as –COOH, –OH, –C–O–C–, and C=O) on graphene sheets. Kumar et al. [24] utilized graphene oxide for the heterogenization of a heteroleptic iridium complex. They targeted –OH and –COOH surface groups of graphene oxide as anchoring sites for the covalent attachment of a Cu–PT complex. We presumed that the stepwise construction of chiral–metal complexes on a graphene oxide(GO) sheet via covalent interaction would overcome the drawbacks of the existing heterogenized catalysts. Herein, we prepared a [RuCl<sub>2</sub>( $\eta^6$ -*p*-cymene)]/chiralthiourea ligand heterogenized on graphene oxide via covalent interaction. The structure of the resultant heterogenized catalyst (G-CLRu(II)) was characterized by means of high-resolution transmission electron microscopy and selected area electron diffraction (HRTEM-SAED), scanning electron microscopy (SEM), energy dispersive spectroscopy (EDS), inductively coupled plasma-mass spectrometry (ICP-MS), Fourier-transform infrared spectroscopy (FT-IR), ultraviolet–visible spectroscopy (UV-Vis), cyclic voltammetry (CV), Raman, nuclear magnetic resonance (NMR), and X-ray photoelectron spectroscopy (XPS). After being characterized, G-CLRu(II) was used for the asymmetric transfer hydrogenation of ketones. Recovery, reusability, and stability of G-CLRu(II) were studied. A possible mechanism is proposed for the G-CLRu(II)-catalyzed asymmetric hydrogenation reaction.

## 2. Results and Discussion

### 2.1. Characterization of G-CLRu(II)

As shown in Scheme 1, [RuCl<sub>2</sub>( $\eta^6$ -*p*-cymene)]/chiralthiourea ligand was attached to graphene nanosheets (G-CLRu (II)) via covalent interactions. Five simple consecutive steps were involved in the stepwise wet synthesis of G-CLRu(II). Coordination mode and covalent bonding involved

in the G-CLRu(II) structure were confirmed by means of various microscopic and spectroscopic techniques. Figure 1 and Figure S1 (Supplementary Materials) show the HRTEM images of G-CLRu(II) and its corresponding SAED pattern. The high-resolution TEM images revealed that the surface of G-CLRu(II) is very smooth without Ru nanoparticles on the surface of graphene oxide. However, the EDS spectrum and the corresponding elemental mapping confirmed the existence of a significant amount of Ru (1.97 wt%). The exact Ru content (1.83 wt%) was determined by digestion of G-CLRu(II) in hot HCl/HNO<sub>3</sub> followed by ICP-MS analysis. In addition to Ru, other elements such as C (67.56 wt%), O (23.79 wt%), S (1.99 wt%), Cl (3.59 wt%), N (1.32 wt%), and Ru (1.75 wt%) were also found in G-CLRu(II) (Figure 1 and Figure S1 in Supplementary Materials). The SAED pattern confirmed the amorphous nature of G-CLRu(II). It can be concluded that there is no reduction of [RuCl<sub>2</sub>(η<sup>6</sup>-*p*-cymene)]/chiralthiourea ligand to Ru nanoparticles on the surface of the graphene sheet. Most of the existing heterogenized catalysts are highly limited due to the reduction/decomposition of the metal-centered ligand to corresponding nanoparticles on the solid support. For example, Sabater et al. [25] immobilized a NHC–Pd(II) complex on graphene oxide via non-covalent interaction. However, they observed a partial decomposition of the NHC–Pd(II) complex to Pd nanoparticles on the surface of graphene oxide. Similarly, Movahed et al. [26] also noticed the similar phenomenon when N-heterocyclic carbene–Pd complex was supported on graphene oxide via covalent interaction. In spite of that, the heterogenized catalysts showed high conversions in alkene hydrogenation, nitro reduction, oxidation of alcohols, and Suzuki coupling reactions. However, the decomposition of metal-centered ligand to nanoparticles could significantly reduce the selectivity of the product. More importantly, this type of heterogenized catalysts is not suitable for enantioselective synthesis. In the present case, no decomposition of [RuCl<sub>2</sub>(η<sup>6</sup>-*p*-cymene)]/chiralthiourea ligand to Ru nanoparticles was observed.



Scheme 1. Preparation of heterogenized chiralcatalyst, G-CLRu(II).

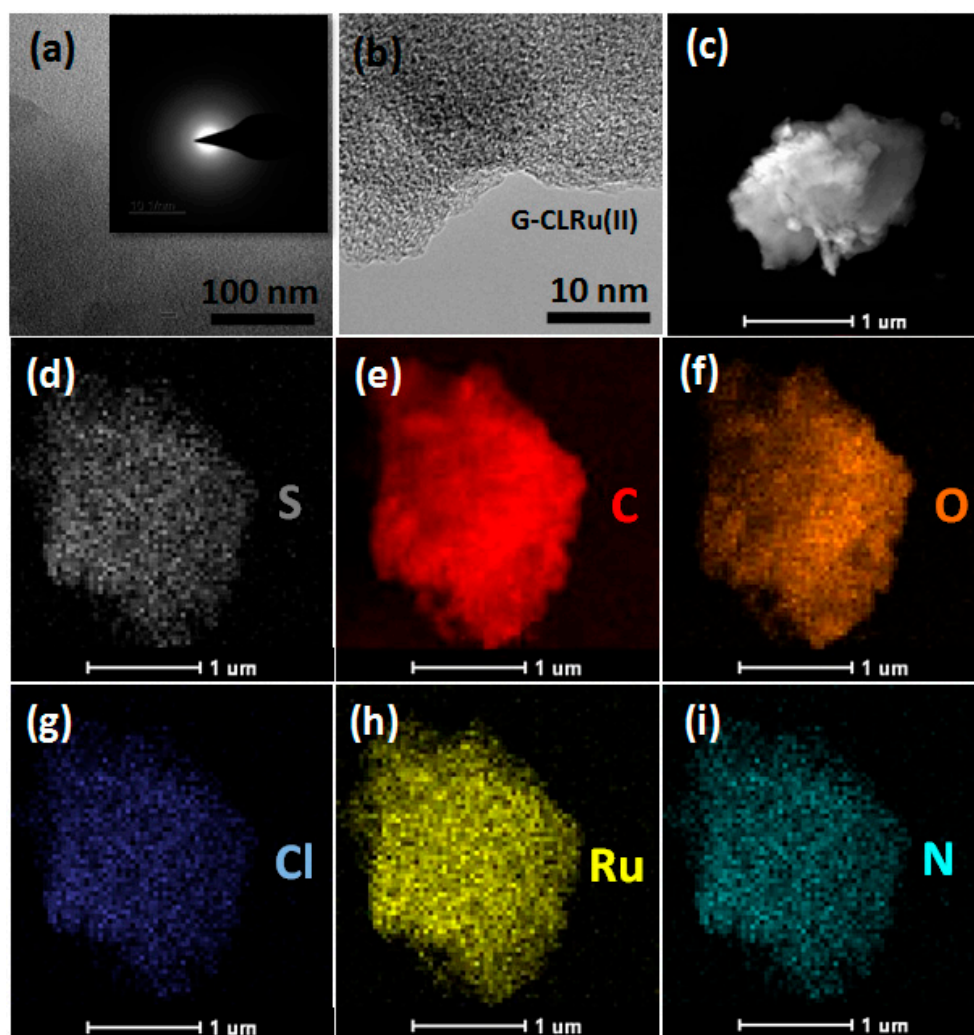


**Figure 1.** (a–c) HRTEM images of G-CLRu(II) and the inset image (a-1) is the corresponding selected area electron diffraction(SAED) pattern, and the corresponding elemental mapping of (d) S, (e) C, (f) O, (g) Cl, (h) Ru, and (i) sulphur (S).

SEM images and corresponding EDS spectrum were taken for G-CLRu(II) (Figure 2). The EDS spectrum of G-CLRu(II) showed the existence of C (66.48 wt%), O (25.47 wt%), S (2.05 wt%), Cl (2.95 wt%), N (1.08 wt%), and Ru (1.97 wt%). The elemental mapping showed that there were no other elements except C, O, N, S, Cl, N, and Ru, indicating that the preparation method is reliable. Moreover, the mapping results proved the uniform grafting of  $[\text{RuCl}_2(\eta^6\text{-}p\text{-cymene})]$ /chiralthiourea ligand on graphene oxide.

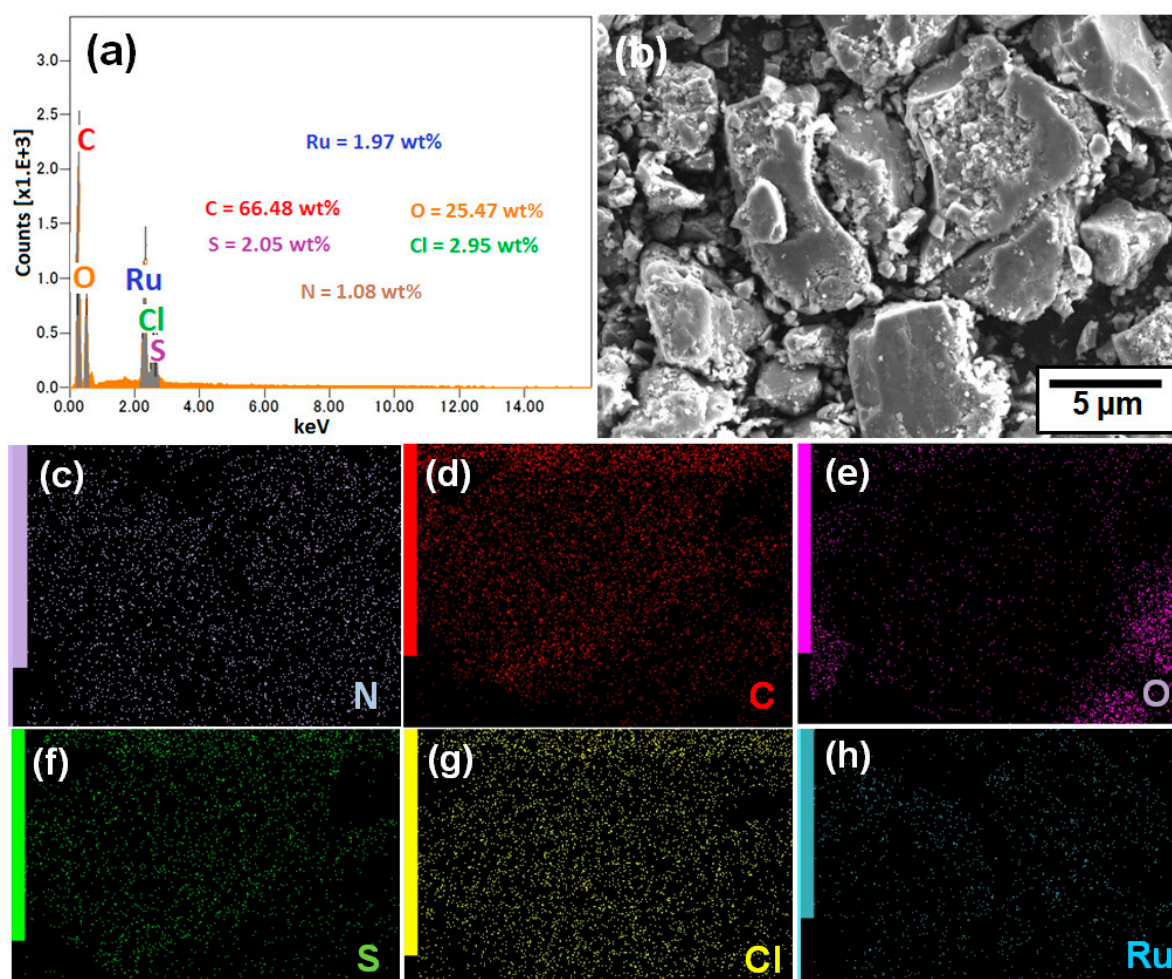


**Figure 2.** (a) EDS spectrum and (b) SEM image of G-CLRu(II), and the corresponding elemental mapping of (c) N, (d) C, (e) O, (f) S, (g) Cl, and (h) Ru.

The formation of the Ru(II)center containing chiral thiourea ligand on graphene oxide was confirmed by various spectroscopic techniques. In particular, the coordination mode and covalent bonding involved in the G-CLRu(II) structure were investigated in detail. Figure 3a shows the UV-Vis spectra of G-COOH, G-COCl, G-CONCS, G-CL, and G-CLRu(II) (Figure 3a). The UV-Vis spectrum of G-COOH showed two distinct absorption peaks at around 215 nm and 270 nm which can be ascribed to  $\pi-\pi^*$  transition of the C=C bond and to  $n-\pi^*$  transition of the  $-\text{COO}^-$  groups, respectively [27]. However, the UV-Vis spectrum of G-COCl showed very weak absorption bands at  $\sim 215$  nm and  $\sim 270$  nm, which may be due to the conversion of the  $-\text{COOH}$  group to  $-\text{COCl}$ . Similarly, the UV-Vis spectra of G-CONCS and G-CL depicted weak absorption bands in the range of 210–330 nm and 450 nm, which confirms the covalent grafting of chiral thiourea ligand on graphene nanosheets. G-CLRu(II) showed four intense peaks at around 230 nm ( $\pi-\pi^*$  transition of the C=C bond), 284 nm ( $n-\pi^*$  transition of the C=O group), 338 nm ( $S(p\pi) \rightarrow M(d\pi)$  ( $M = \text{Ru}^{2+}$ ) LMCT transition), and 441 nm (d-d transition band) [28]. The results confirm the formation of the Ru complex with graphene oxide.

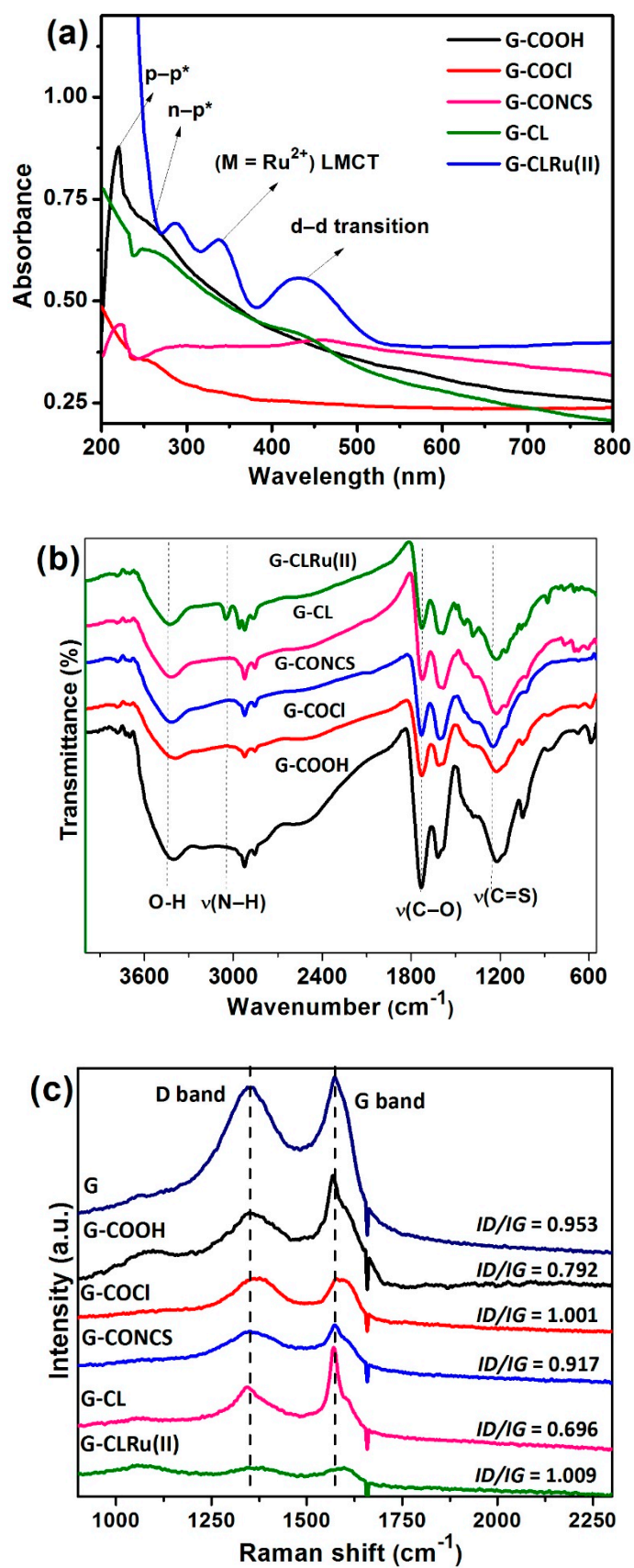


**Figure 3.** (a) Ultraviolet–visible spectroscopy (UV-Vis) spectra, (b) Fourier-transform infrared spectroscopy (FT-IR) spectra, and (c) Raman spectra of G-COOH, G-COCl, G-CONCS, G-CL, and G-CLRu(II).

Figure 3b shows the FT-IR spectra of G-COOH, G-COCl, G-CONCS, G-CL, and G-CLRu(II) (Figure 3b). The FT-IR spectrum of G-COOH showed characteristic features in the regions,  $3430\text{ cm}^{-1}$  for  $\nu(\text{O-H})$ ,  $1725\text{ cm}^{-1}$  for  $\nu(\text{C=O})$  from the C=O and COOH groups,  $1380\text{ cm}^{-1}$  for  $\nu(\text{C-OH})$ , and  $1027\text{ cm}^{-1}$   $\nu(\text{C-O})$ . In addition, the peaks at around  $1639\text{ cm}^{-1}$  were ascribed to the skeletal vibrations from unoxidized graphitic domains and the peak at  $\sim 2900\text{ cm}^{-1}$  corresponds to aromatic  $\nu(\text{C-H})$  bonds of graphene oxide. In comparison to G-COOH, the FT-IR spectra of G-CL and G-CLRu(II) changed slightly (including new peaks, peak shifting, and variations in the peak intensities), which is due to the attachment of the chiral-Ru complex to the surface of graphene oxide [29,30]. The FT-IR spectra of G-CL showed peaks at  $3076\text{--}3312$ ,  $1698\text{--}1725$ , and  $1256\text{--}1271\text{ cm}^{-1}$  that were assigned to  $\nu(\text{N-H})$ ,  $\nu(\text{C-O})$ , and  $\nu(\text{C=S})$ , respectively. On complexation, the peaks of  $\nu(\text{N-H})$  and  $\nu(\text{C=O})$  were observed to be unchanged, whereas the peak at  $1256\text{--}1271\text{ cm}^{-1}$   $\nu(\text{C=S})$  shifted towards higher frequencies, indicating the sulfur-only coordination mode of the chiral thiourea ligands [31]. In addition, FT-IR spectra of both G-CL and G-CLRu(II) showed new peaks at  $697$ ,  $851$ ,  $1467$ , and  $1505\text{ cm}^{-1}$ , which corresponds to absorptions of the benzene ring of the chiral ligand segments [30].

Raman spectra were recorded for the fresh G, G-COOH, G-COCl, G-CONCS, G-CL, and G-CLRu(II) in order to study the chemical and structural changes before and after Ru complex grafting (Figure 3c). Characteristic G-band and D-band lines were observed for all the five samples. The D-band line ( $\sim 1355\text{ cm}^{-1}$ ) is related to the amount of defect sites, whereas the G-band line ( $\sim 1570\text{ cm}^{-1}$ ) is associated with the vibrations of  $\text{sp}^2$ -bonded carbon networks [32]. The ID/IG ratio was calculated from the intensities of G-band and D-band lines for all the five samples (Figure 3c). In comparison to G-COOH (0.792), the ID/IG ratios of G-COCl and G-CONCS were calculated to be high. The increase in the ID/IG ratio is mainly due to the formation of more defects in the graphene planes [32]. The ID/IG ratio of 0.696 was calculated for G-CL, whereas, after complexation, the value significantly increased to 1.009. In the present case, the formation of defects is only due to the covalent grafting of Ru(II)-chiral thiourea ligands on graphene oxide.

The formation of the Ru(II)-chiral complex with the graphene nanosheet was further analyzed by  $^1\text{H}$  and  $^{13}\text{C}$  NMR spectra (see Figures S8–S13 in Supplementary Materials). Figure 4 shows the chemical shift values in ppm ( $^1\text{H}$  and  $^{13}\text{C}$  NMR) observed for the  $[\text{RuCl}_2(\eta^6\text{-}p\text{-cymene})]$ /chiral thiourea ligand covalently bonded to graphene nanosheets. As noted in Figure 4, the significant signals were clearly observed (see NMR spectra in Supplementary Materials). In the  $^1\text{H}$  NMR spectrum of G-CLRu(II), the signals corresponding to *p*-cymene are clearly seen at 1.20 ppm (singlet,  $2\text{CH}_3$  of *p*-cymene), 2.37 ppm (multiplet,  $\text{CH}_3$  of *p*-cymene), 2.97 ppm (multiplet, CH of *p*-cymene), and 5.20–5.40 ppm (multiplet, aromatic protons of *p*-cymene). Similarly, the signals corresponding to chiral Ru(II) complex are observed at 1.48 ppm (doublet,  $\text{CH}_3$  of the chiral thiourea ligand), 4.32 ppm (multiplet, asymmetric hydrogen), 8–7 ppm (multiplet, aromatic protons of the chiral thiourea ligand), 8.20 ppm (singlet, C=S attached N-H), and 13.82 ppm (singlet, C=O and C=S attached N-H). The graphene oxide ring protons are observed at 8–7, 5–6, and 2–3 ppm. The  $^{13}\text{C}$  NMR showed signals at 18.33 ( $\text{CH}_3$  of *p*-cymene), 20.87 ( $\text{CH}_3$  of the ligand), 21.13 ( $2\text{CH}_3$  of *p*-cymene), 30.45 (CH of *p*-cymene), 57.62 (asymmetric carbon), 85–87 (aromatic carbons of *p*-cymene), 100.57 and 106.86 (quaternary carbons of *p*-cymene), 125–130 ppm (CH), 170.12 (C=O), and 186.74 (C=S). The chemical shift values observed were consistent with the literature values [9,20,29,33,34].

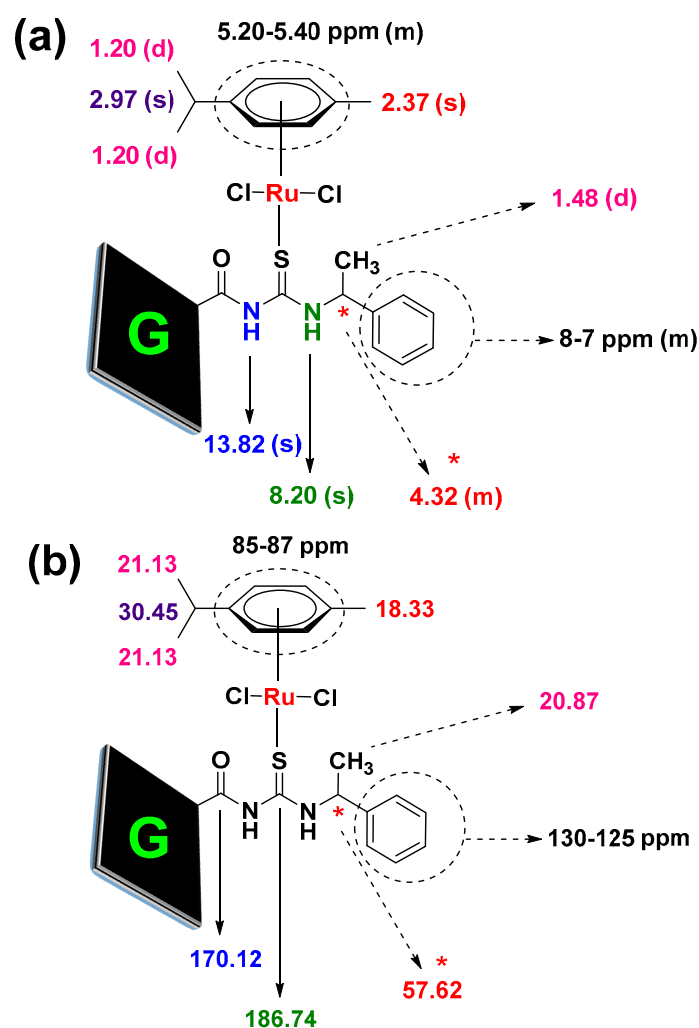


**Figure 4.** Molecular structure of [RuCl<sub>2</sub>(η<sup>6</sup>-*p*-cymene)]/chiralthiourea ligand covalently bonded to graphene nanosheets; (a) <sup>1</sup>H NMR chemical shift values and (b) <sup>13</sup>C NMR chemical shift values (signals observed).

In order to investigate the redox behavior and stability of G-CLRu(II), CV curves were recorded. Figure 5 shows the CV curves of G-Cl and G-CLRu(II) recorded in MeCN containing tetrabutylammonium perchlorate at a potential range 0 to +2.0 V with a scan rate of 100 mV·s<sup>-1</sup>. In general, the Ru complexes possibly undergo one-electron redox reaction between Ru(II) and Ru(III). The present G-CLRu(II) shows quasi-reversible ( $I_{pa}/I_{pc} = 1$ ) (at 0.57 vs. SCE) waves corresponding to the one-electron oxidation of Ru(II) to Ru(III) (Figure 5a) [35]. The waves corresponding to Ru(II)  $\rightleftharpoons$  Ru(III) interconversion are highly reproducible as quasi-reversible at different scans and concentrations (Figure 5b). However, there are no additional peaks observed for other samples, such as G-COOH, G-COCl, G-CONCS, and G-Cl (data not shown). It is proved that the higher redox potential indicates the good stability of the complexes, whereas the lower redox potential of the complex should increase the interconversion [35]. The higher redox potential observed for the present G-CLRu(II) confirmed the greater stability of the Ru(II) complexes upon coordination of the chiral thiourea ligand [35,36].

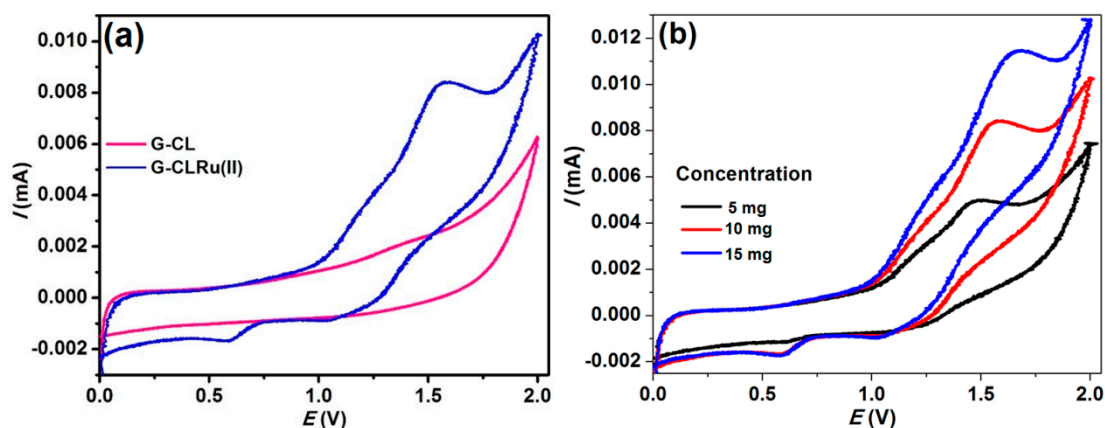
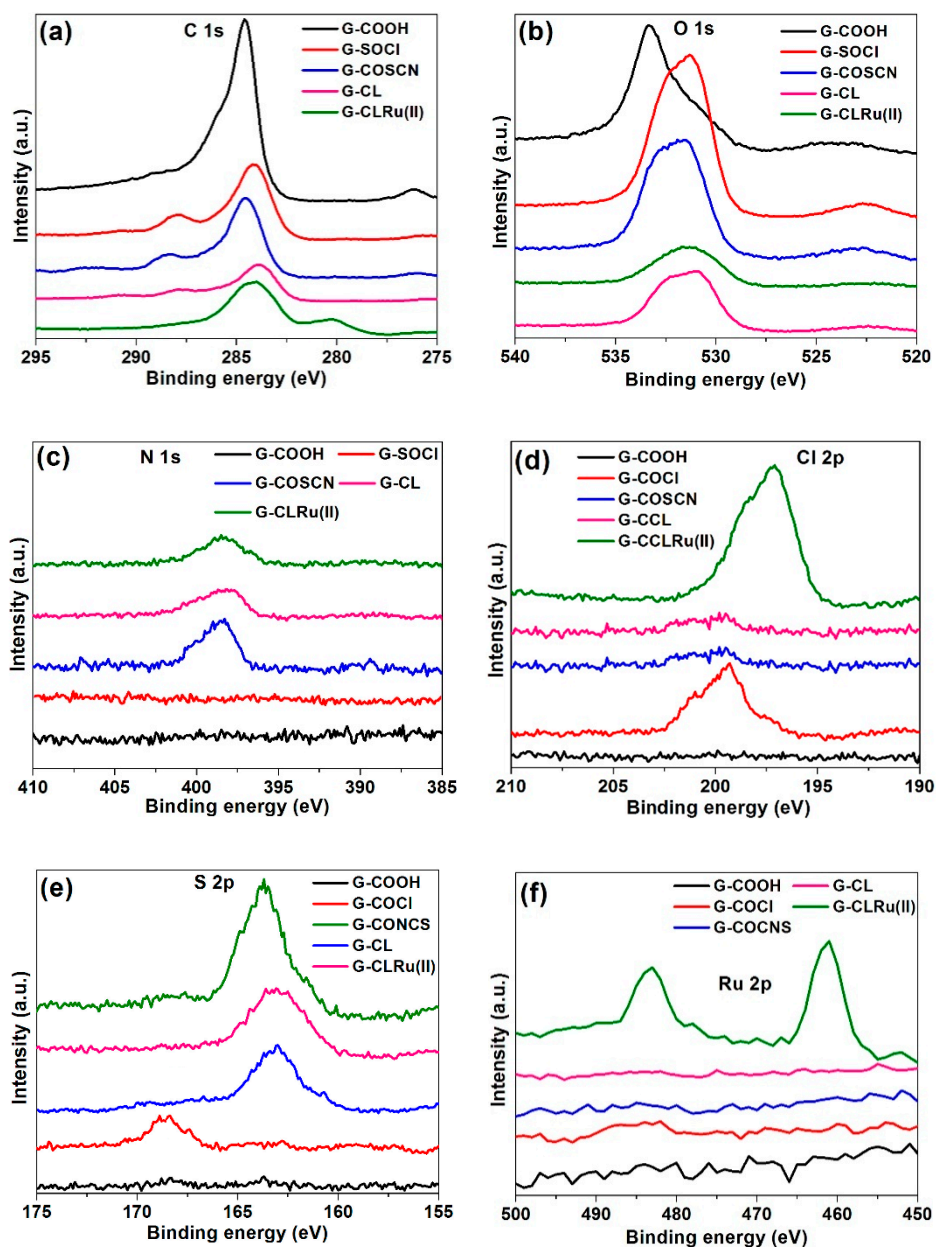


**Figure 5.** (a) Cyclic voltammograms of G-Cl and G-CLRu(II), (b) cyclic voltammograms of G-CLRu(II) at different concentrations.

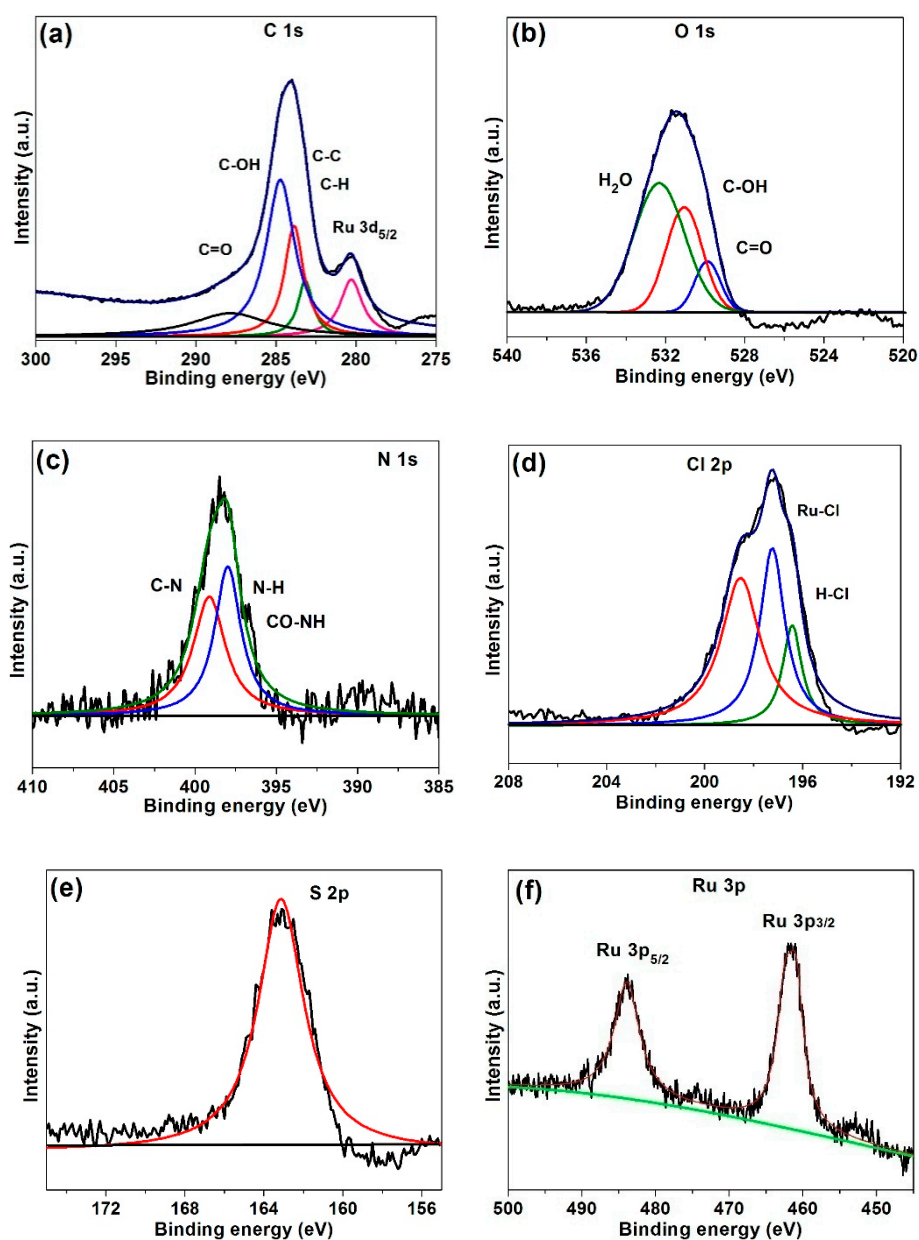
XPS spectra were recorded for all five samples (G-COOH, G-COCl, G-CONCS, G-Cl, and G-CLRu(II)) (Figures 6 and 7, and Figures S2–S6 in Supplementary Materials). The survey spectra of all five samples are shown in Figure S2 (see Supplementary Materials). For all five samples, two characteristic peaks, C 1s and O 1s, were observed at around 285 and 532 eV, respectively. In order to study the functional groups bonded to the surface of graphene oxide, curve fitting was performed for selected XPS peaks using Gaussian–Lorentzian peak shape after a Shirley baseline correction. The deconvoluted XPS C 1s peak of G-COOH showed four intense peaks at around 284–285 eV (C–C and C–H), 285.4 (C–OH), 286.7 (C=O), and 288.2 eV (–COOH) (Figure S3 in Supplementary Materials) [37]. Similarly, the deconvolution of O 1s peak of G-COOH resulted in four peaks located at 530.2, 531.2, 532.4, and 534.2 eV, which were assigned to C=O, –COOH, C–OH, and H<sub>2</sub>O (Figure S3 in Supplementary Materials) [38]. The results indicate that the G-COOH has a –COOH group attached to the surface of graphene oxide. The G-COCl showed a Cl peak at 199.6 eV, which indicates the conversion of acid (–COOH) to acid chloride (–COCl) (Figure S4 in Supplementary Materials) [39]. The XPS spectrum of G-COCl after treatment with KSCN showed two new peaks at around 162.6 eV (S 2p) and 397.8 eV (N 1s), while the peak corresponding to Cl 2p (199.6 eV) completely disappeared (Figure 6d). This clearly indicates the replacement of –Cl from –COCl with the thiocyanate group (–SCN) (Figures S4 and S5 in Supplementary Materials). The XPS spectrum of G-Cl showed peaks in four different regions, such as C 1s (285 eV), O 1s (531 eV), N 1s (398 eV), and S 1s (163 eV). In comparison to the other four samples (G-COOH, G-COCl, G-CONCS, and G-Cl), G-CLRu(II) showed new peaks in the Ru 2p region (Ru 3p<sub>3/2</sub> = 461.5 eV and Ru 3p<sub>5/2</sub> = 484.5 eV) (Figure 6f) [38]. Similarly, G-CLRu(II) showed an intense new peak in the Cl 2p region (199.6 eV) attributed to the Cl–Ru–Cl group [40]. In order to understand the coordination of Ru, the peak position of N 1s, S 1s, and O 1s of G-CLRu(II) was compared with G-Cl. It can be seen that the peak position of S 1s is significantly shifted towards higher binding energy (from 162.5 eV to 164.1 eV), whereas the N 1s and O 1s peak positions (398 eV and 531 eV) were observed to be unchanged, which indicates the monodentate neutral coordination of the S atom to the Ru.

The XPS spectrum of G-CLRu(II) was investigated in detail by deconvoluting the C 1s, O 1s, N 1s, Cl 2p, S 2p, and Ru 2p peaks (Figure 7). The deconvolution of the C 1s peak resulted in four peaks at 283.5–284.1 eV (C–C and C–H), 284.9 eV (C–OH), and 287.5 eV (C=O). In addition, a weak peak at 280.3 eV is attributed to the Ru (+2) (Figure 7a) [39]. Investigating the positions of the deconvoluted C 1s peaks confirmed the presence of C–OH and C=O groups in the G-CLRu(II) structure. Interestingly, the N 1s peak was deconvoluted into two intense peaks at 397.7 (–CONH) and 398.1 eV (C=O and C=S attached N–H) [41,42]. The Cl 2p peak fitting resulted in three obvious peaks at 196.3 (HCl), 197.3 (Cl–Ru–Cl) and 198.3 eV (Figure 7d) [39]. The S 2p peak at 164.2 eV may be due to the photoemission from the C=S group [41]. The new peaks in the Ru 2p region at 461.5 eV (Ru

$3p_{3/2}$ ) and 484.5 eV ( $Ru\ 3p_{5/2}$ ) were observed for G-CLRu(II) [43]. In addition, the deconvoluted C 1s peak at 280.1 eV ( $Ru^{II}\ 3d_{5/2}$ ) confirms the presence of the Ru(II) center in the G-CLRu(II) structure (Figure 7a) [44,45]. Overall, the results confirmed that the  $[RuCl_2(\eta^6-p\text{-cymene})]$ /chiralthiourea ligand was constructed on the graphene nanosheet. The coordination mode and covalent bonding involved in the G-CLRu(II) structure were also verified.



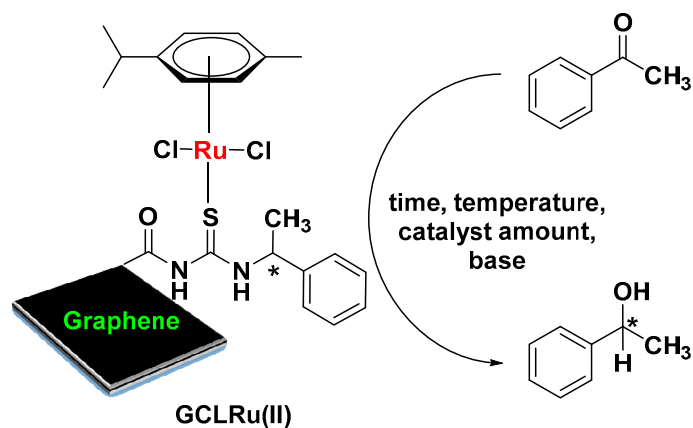
**Figure 6.** X-ray photoelectron spectroscopy(XPS) spectra of G-COOH, G-COCl, G-CONCS, G-CL, and G-CLRu(II): (a) C 1s, (b) O 1s, (c) N 1s, (d) Cl 2p, (e) S 2p, and (f) Ru 2p peaks.



**Figure 7.** XPS spectra of G-CLRu(II): deconvoluted (a) C 1s, (b) O 1s, (c) N 1s, (d) Cl 2p, (e) S 2p, and (f) Ru 2p peaks.

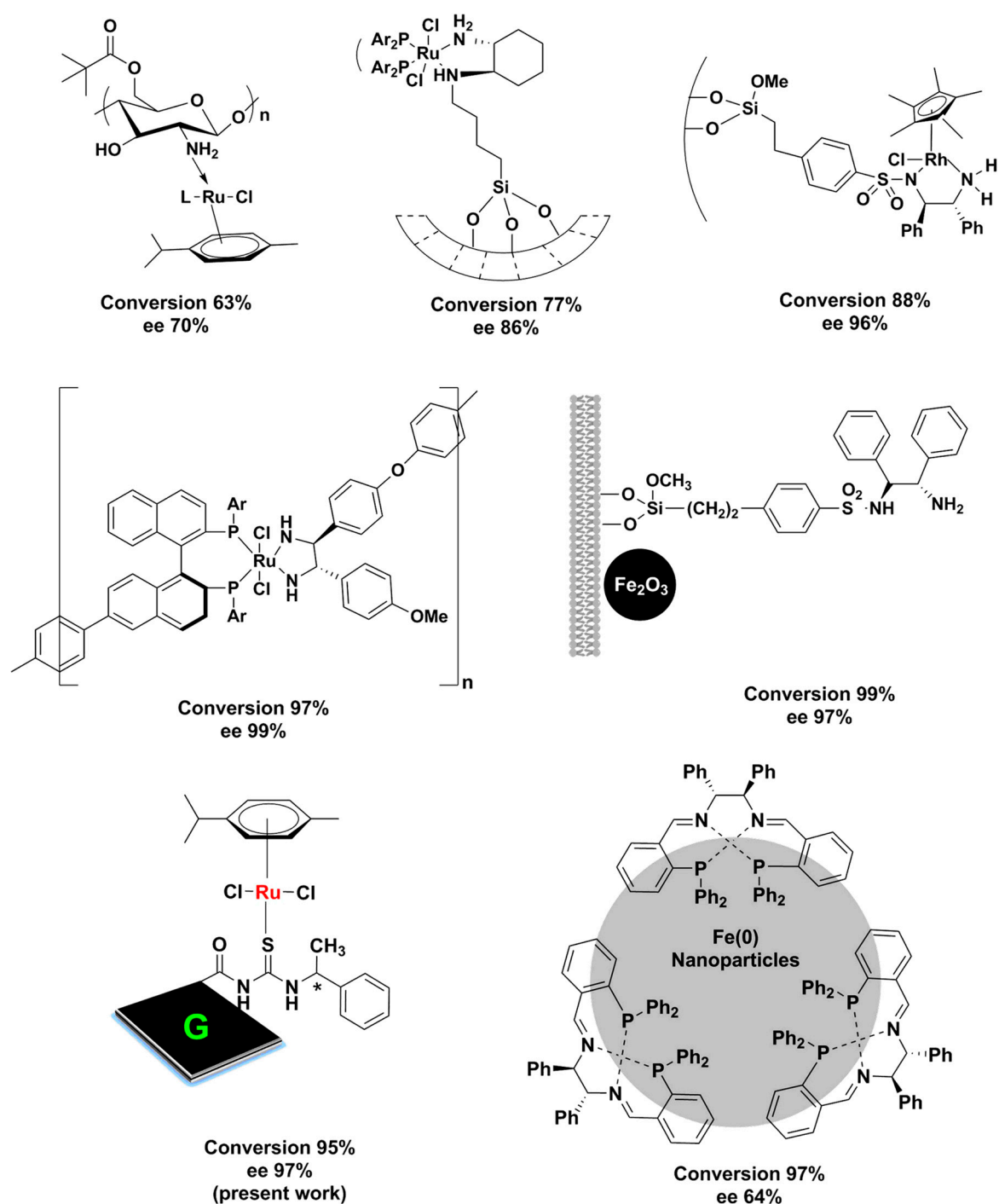
## 2.2. Asymmetric Transfer Hydrogenation of Ketones

After being characterized, G-CLRu(II) was used as catalyst for the asymmetric transfer hydrogenation of ketones. To the best of our knowledge, this is one of the best heterogenized chiral catalysts reported for the asymmetric transfer hydrogenation of ketones. The reduction of acetophenone to 1-phenylethanol in 2-propanol was employed as a model reaction (Table 1). It was found that the activity and stability of the present G-CLRu(II) are highly influenced by the reaction condition. Catalyst amount, base, temperature, and time were screened to find out the most suitable reaction conditions. A trace amount of the desired product, 1-phenylethanol, was observed when a reaction mixture (acetophenone (1 mmol), 2-propanol (5 mL) and KOH (1 mmol)) was refluxed in the absence of G-CLRu(II) for 24 h (Table 1, entry 1). Similarly, the fresh graphene was found to be inactive in the reduction reaction. The reaction performed in the presence of G-CLRu(II) showed a high yield of 95%. The ee was calculated to be 97% and the absolute configuration was determined to be *S*. Interestingly, the graphene impregnated with [RuCl<sub>2</sub>(η<sup>6</sup>-*p*-cymene)]/chiralthiourea ligand (non-covalently attached) showed similar yields; however, the reusability of the catalyst was found to be very low due to leaching of the catalysts. A 5 mg amount of G-CLRu(II) was found to be not enough since it gave only 43% of the desired product (Table 1, entry 2). The optimum amount of G-CLRu(II) was 10 mg, while increasing the amount of G-CLRu(II) showed no improvement in the yield (Table 1, entries 3 and 4). Choosing a suitable base is very important in this catalytic system. Among three different bases (KOH, NaOH, and (CH<sub>3</sub>)<sub>3</sub>COK) tested, KOH was found to be the best one (yield of 95% and ee of 97%) (Table 1, entries 3, 5, and 6). The use of NaOH or (CH<sub>3</sub>)<sub>3</sub>COK showed a better 99% yield of the product (Table 1, entries 5 and 6); however, the ee values were found to be low (about 60%) when compared to the reaction carried out using KOH. It was found that the temperature also played a crucial role in this catalytic system. The model reaction was performed at four different temperatures (27, 50, 70, and 82 °C) (Table 1, entries 3, 7–9). The reaction required a reflux temperature of 82 °C to achieve the maximum yield of 95% with 95% ee. Subsequently, reaction time was also optimized (Table 1, entries 10–15). This catalytic system yielded 95% of the desired product after the reaction was stirred for 24 h. Overall, stirring the mixture of 10 mg of G-CLRu(II), 1 mmol of acetophenone, 1 mmol of KOH, and 5 mL of 2-propanol at 82 °C for 24 h yielded 95% of the desired product with 97% ee. The turnover number (TON) and turnover frequency (TOF) values were also calculated (TON = (molar amount of product)/(molar amount of active sites), and TOF = TON/(time in h)). Remarkably very high TON and TOF values of 524.9 and 21.9 h<sup>-1</sup> were obtained for the present G-CLRu(II) system. However, the heterogenized polyligand/[Ru(*p*-cymene)Cl<sub>2</sub>] catalyst yielded 63% of the desired product with 70% ee [13]. Similarly, Ru(II)-chiral complex-supported mesoporous silica nanosphere (MSN-48) gave only 77% of the product with 86% ee [11]. Similarly, this catalytic system is found to be better in comparison to previously reported heterogenized catalysts (see Scheme 2) [46–52]. In the present case, π-stacking interactions with the graphene sheets might have provided further π-delocalization that improved the activity of the [RuCl<sub>2</sub>(η<sup>6</sup>-*p*-cymene)]/chiralthiourea ligand covalently bonded to graphene nanosheets (G-CLRu(II)).

Table 1. Standardization of reaction conditions <sup>a</sup>.

Serial No.	Catalyst, Amount (mg)	Base	Temperature (°C)	Time (h)	Yield (%) <sup>b</sup>	ee (%) <sup>c</sup>
1	0	KOH	82	24	12	-
2	G-CLRu(II), 5	KOH	82	24	43	95
3	G-CLRu(II), 10	KOH	82	24	95	97
4	G-CLRu(II), 15	KOH	82	24	95	96
5 <sup>d</sup>	G-CLRu(II), 10	NaOH	82	24	99	83
6 <sup>d</sup>	G-CLRu(II), 10	(CH <sub>3</sub> ) <sub>3</sub> COK	82	24	99	89
7	G-CLRu(II), 10	KOH	27	24	9	-
8	G-CLRu(II), 10	KOH	50	24	23	93
9	G-CLRu(II), 10	KOH	70	24	47	95
10	G-CLRu(II), 10	KOH	82	2	9	-
11	G-CLRu(II), 10	KOH	82	4	18	92
12	G-CLRu(II), 10	KOH	82	8	36	94
13	G-CLRu(II), 10	KOH	82	12	45	97
14	G-CLRu(II), 10	KOH	82	16	64	95
15	G-CLRu(II), 10	KOH	82	20	88	95

<sup>a</sup> Reaction conditions: acetophenone (1 mmol), 2-propanol (5 mL), and base (1 mmol). <sup>b</sup> GC yield. <sup>c</sup> The ee was determined by chiral HPLC. <sup>d</sup> Catalyst was not stable.



**Scheme 2.** Activity of reported heterogenized chiral catalysts for the asymmetric transfer hydrogenation of ketones [11,13,41–47].

The present G-CLRu(II) was used to catalyze the 1-(3-nitrophenyl)ethan-1-one, 3-acetylpyridine, and (4-fluorophenyl)(phenyl)methanone under the optimized reaction conditions. The reduction of 1-(3-nitrophenyl)ethan-1-one, 3-acetylpyridine, and (4-fluorophenyl)(phenyl)methanone by G-CLRu(II) produces the corresponding chiral alcohols in good yields with maximum ee % and TON/TOF values. The absolute configuration determined from the optical rotation values was *S* for all four products ((*S*)-1-phenylethan-1-ol, (*S*)-1-(3-nitrophenyl)ethan-1-ol, (*S*)-1-(pyridin-3-yl)ethan-1-ol, and (4-fluorophenyl)(phenyl)methanol). Under the optimized reaction conditions, G-CLRu(II)

produced (*S*)-1-(3-nitrophenyl)ethan-1-ol in a 97% yield with very high 99% ee and TON/TOF values of 535.9/22.3 h<sup>-1</sup>. The reduction of 3-acetylpyridine produced (*S*)-1-(pyridin-3-yl)ethan-1-ol in a 97% yield with very high 99% ee and TON/TOF values of 535.9/22.3 h<sup>-1</sup>. Similarly, an 89% yield of (4-fluorophenyl)(phenyl)methanol with high ee of 93% was obtained from the G-CLRu(II)-catalyzed asymmetric transfer hydrogenation of (4-fluorophenyl)(phenyl)methanone. The TON/TOF values were calculated as 491.7 and 20.5 h<sup>-1</sup>. Aliphatic ketones such as hexan-2-one and octan-2-one were also transformed to the corresponding alcohols. The reduction of hexan-2-one produced hexan-2-ol in a 79% yield with ee of 91% (TON of 436.5 and TOF of 18.1 h<sup>-1</sup>). Similarly, a 67% yield of octan-2-ol with ee of 83% was obtained by the reduction of octan-2-one in the presence of G-CLRu(II). The TON/TOF values of 370.2/15.4 h<sup>-1</sup> were obtained. Both hexan-2-ol and octan-2-ol possess the *S* configuration. The catalytic activity of the present G-CLRu(II) was compared with that of already reported heterogenized chiral ligands (Scheme 2). It can be seen that most of the heterogenized catalysts are silica-based systems. Very few reports deal with the role of magnetic nanoparticles and biopolymers (like chitosan) as a platform for the heterogenization of active chiral catalysts. In spite of the unique physicochemical properties, graphene oxide has not been much studied for enantioselective heterogeneous catalysis. To the best of our knowledge, this is the first efficient and stable graphene-based heterogenized Ru(II)-chiral catalyst for the asymmetric transfer hydrogenation of ketones.

A possible mechanism is proposed for the transfer hydrogenation of acetophenone catalyzed by G-CLRu(II) (Figure 8). In the first step, the reaction between G-CLRu(II) and 2-propanol in the presence of KOH (1) forms a Ru-alkoxide active species (2) and subsequently generates an 18-electron Ru-hydride intermediate via intramolecular hydrogen transfer. Subsequently, in the second step, the Ru-hydride species interacts with acetophenone through Ru-H and N-H units to form a six-membered transition state (3) (follow Noyori's outer-sphere mechanism) [53]. Finally, the corresponding chiral (*S*)-1-phenylethan-1-ol from 3 is obtained.

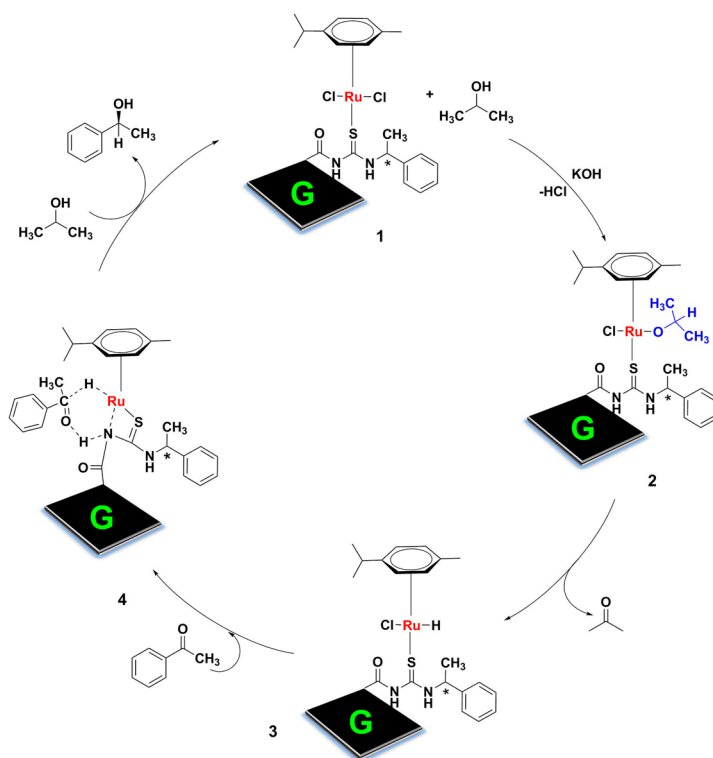


**Figure 8.** Proposed mechanism for the transfer hydrogenation of acetophenone catalyzed by G-CLRu(II).

### 2.3. Recovery, Reusability, and Stability

The most challenging properties of heterogenized catalysts to be achieved are recovery, stability, and reusability. In order to confirm the stability of the present G-CLRu(II), a hot filtration test was carried out. In the typical hot filtration test, a mixture of G-CLRu(II) (10 mg), acetophenone (1 mmol), KOH (1 mmol), and 2-propanol (5 mL) was stirred at 82 °C for 12 h [34]. Subsequently, the catalyst was recovered from the reaction mixture by centrifugation and the filtrate was continually stirred for another 12 h. The reaction mixture was tested by GC and ICP-MS analysis. The yield of the desired product was determined to be 45% and the ICP-MS result showed that there was no Ru content in the reaction mixture (Figure 9). In addition, the recovery percentage of the G-CLRu(II) was found to be over 95% (about 9.5 mg of G-CLRu(II) was recovered from 10 mg of the reaction mixture). Moreover, the filtrate stirred for 12 h also showed no significant increase in the yield of the product. The results confirmed that the G-CLRu(II) is stable and easily recoverable.

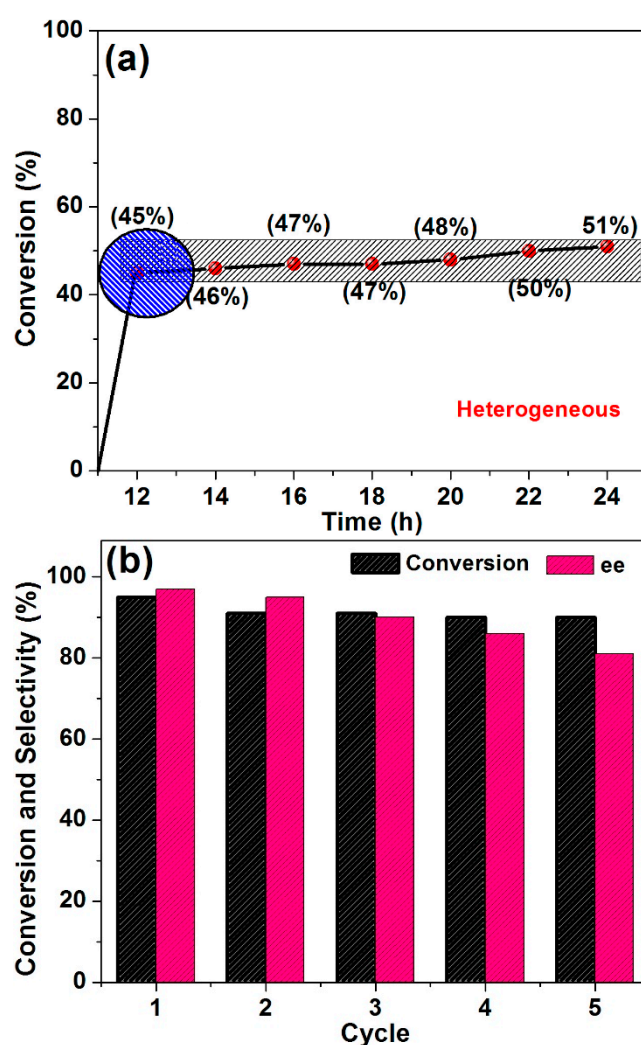


Figure 9. (a) Heterogeneity and (b) reusability of G-CLRu(II).

Most of the heterogenized catalysts suffer from poor reusability and selectivity due to their instability under various reaction conditions. In fact, the reduction of metal–ligand to nanoparticles on the solid support is observed to be the major possible reason for this issue. This catalytic system showed good reusability even after the fifth use. G-CLRu(II) can be used for at least five cycles without significant loss in its catalytic activity. At the second cycle, G-CLRu(II) showed 93% of the desired product and the ee was calculated to be 95%. It was observed that the yield of the product was

maintained but that the ee was slightly decreased after the fifth cycle. G-CLRu(II) after the fifth cycle use was tested by HRTEM imaging. The result showed no particle formation (Figure S7 in Supplementary Materials). Overall, G-CLRu(II) is highly recoverable, stable, and reusable. Indeed, the stepwise synthesis of the present G-CLRu(II) is the key factor for the good stability and recovery, thus showing great potential practical applications.

### 3. Experimental Section

#### 3.1. Materials

High purity graphene oxide (GO) was purchased from ACS Materials, Pasadena, CA, USA. Thionyl chloride ( $\text{SOCl}_2$ ), acids ( $\text{H}_2\text{SO}_4$  and  $\text{HNO}_3$ ), and bases (KOH, NaOH, and  $(\text{CH}_3)_3\text{COK}$ ) were received from Wako Pure Chemicals, Osaka, Japan. Acetophenone, potassium thiocyanate (KSCN), (S)-(-)-1-phenylethylamine,  $[\text{RuCl}_2(\eta^6\text{-}p\text{-cymene})]_2$ , 3-acetylpyridine, (4-fluorophenyl)(phenyl)methanone, and 2-propanol were purchased from Sigma-Aldrich, St. Louis, Missouri, USA. All the chemicals were used as received. All solvents used were of HPLC grade and were used as received.

#### 3.2. Preparation of G-CLRu(II) Catalyst

The preparation of G-CLRu(II) involved five simple steps as shown in Scheme 1. In the first step, 500 mg of graphene oxide were dispersed in 100 mL of concentrated  $\text{H}_2\text{SO}_4/\text{HNO}_3$  (1:3 ratios) and the resultant mixture was sonicated for 30 min followed by stirring at 60 °C for 6 h. After cooling down to room temperature, the above mixture was diluted with 2 L of distilled water and then vacuum-filtered to obtain COOH-rich graphene oxide (G-COOH). In the second step, the resultant G-COOH (400 mg) was dispersed in 25 mL of DMF containing an equal concentration of  $\text{SOCl}_2$ , and the mixture was stirred at 80 °C for 12 h to obtain G-COCl. The resultant G-COCl was washed well and vacuum-dried. In the third step, a mixture of G-COCl (400 mg), KSCN (10 mmol, 971.81 mg), and acetone (25 mL) was refluxed for 3 h to obtain G-CONCS. Subsequently, in the fourth step, the G-CONCS was reacted with chiral (S)-(-)-1-phenylethylamine (excess amount) dissolved in 25 mL of acetone by magnetically stirring the mixture at 27 °C for 3 h. Finally, about 450 mg of chiral *N*-((1-phenylethyl)carbamothioyl)formamide ligand covalently bonded with graphene sheets (G-CL) were successfully obtained.

In the fifth step, the resultant chiral G-CL ligand (400 mg) was allowed to react with the excess amount of  $[\text{RuCl}_2(\eta^6\text{-}p\text{-cymene})]_2$  in 25 mL of toluene by magnetically stirring the mixture at 27 °C for 6 h. The  $[\text{RuCl}_2(\eta^6\text{-}p\text{-cymene})]$ /chiralthiourea ligand covalently bonded to graphene nanosheets (G-CLRu(II), ~520 mg) was obtained as the final product. The G-CLRu(II) was washed well with toluene, vacuum-dried, and stored under inert atmosphere.

#### 3.3. Characterization of G-CLRu(II)

An HRTEM-SAED (JEOL JEM-2100F, Akishima, Tokyo, Japan) instrument was operated at accelerating voltage of 200 kV to analyze the microstructure of G-CLRu(II). FT-IR (IR Prestige-21, Shimadzu, Kyoto, Japan) and UV-Vis (Shimadzu UV-2600 spectrophotometer (Kyoto, Japan) spectrometers were used to confirm the construction of the Ru(II)-chiralthiourea ligand on graphene oxide. FT-IR spectra in the range 4000–550  $\text{cm}^{-1}$  were recorded with KBr pellets at 2  $\text{cm}^{-1}$  for a minimum of 32 scans. SEM-EDS were performed on a Hitachi 3000H SEM (Chiyoda, Tokyo, Japan) and an ICP-MS (7500CS, Agilent, Santa Clara, CA, USA) was used for determining the Ru-content in G-CLRu(II). Defects in G-CLRu(II) were calculated using Raman spectroscopy (Hololab 5000, Kaiser Optical Systems Inc., Ann Arbor, MI, USA). During the Raman analysis, the Ar laser functioned at 532 nm with a Kaiser holographic edge filter.  $^1\text{H}$  and  $^{13}\text{C}$  NMR spectra were recorded on a Bruker 500 or 400 MHz and 125 or 100 MHz spectrometer (Billerica, MA, USA), respectively. Electrochemical experiments were performed in a BioLogic SP-150 advanced electrochemical system (Miami, FL, USA), using a traditional three-electrode cell assembly with glassy carbon (GC) as working electrode,

saturated calomel electrode (SCE) as reference electrode, and platinum wire as auxiliary electrode. Cyclic voltammograms were recorded at a  $100 \text{ mV}\cdot\text{s}^{-1}$  scan rate. The complexes were dissolved in MeCN containing the necessary amount of tetra butyl ammonium per chlorate [(n-Bu<sub>4</sub>N)(ClO<sub>4</sub>)], used as the supporting electrolyte. XPS spectra were recorded on a Kratos Axis-Ultra DLD device (Kratos Analytical Ltd., Japan). During the XPS analysis, the samples were irradiated with Mg K $\alpha$  ray source. A Shimadzu GC 2010 gas chromatograph (Kyoto, Japan) with a Restek-5 capillary column and a Shimadzu HPLC instrument (Kyoto, Japan) with a Daicel Chiralcel OB-H column were used to study the catalytic performance. A Rudolph Autopol IV polarimeter (Hackettstown, NJ, USA) was used to measure specific rotation values.

### 3.4. Procedure for G-CLRu(II)-Mediated Asymmetric Transfer Hydrogenation

A mixture of G-CLRu(II) (10 mg, 0.181 mol %), acetophenone (1 mmol), KOH (1 mmol), and 2-propanol (5 mL) was magnetically stirred under N<sub>2</sub> atmosphere at 82 °C for 24 h. Progress of the reaction was monitored by GC and the ee values were determined using HPLC with a Chiralcel OB-H column. Prior to the GC and HPLC analysis, G-CLRu(II) was removed from the reaction mixture by centrifugation for the recycle experiment. After completion of the reaction, the reaction mixture was cooled to room temperature and then passed through a short silica gel column with n-hexane/ethyl acetate. <sup>1</sup>H and <sup>13</sup>C NMR spectra were also recorded for the final products. The recovered G-CLRu(II) was washed well with 2-propanol and used for reusability and stability tests.

## 4. Conclusions

In conclusion, [RuCl<sub>2</sub>( $\eta^6$ -*p*-cymene)]/chiralthiourea ligand was constructed on graphene nanosheets by a simple stepwise synthesis. Coordination mode and covalent bonding involved in the G-CLRu(II) structure were supported by spectroscopic techniques. G-CLRu(II) demonstrated good catalytic performance with respect to the asymmetric transfer hydrogenation of ketones (yields of up to 95%, ee of up to 99%, and TON/TOF values of 535.9/22.3 h<sup>-1</sup>). To the best of our knowledge, this is one of the best heterogenized catalysts reported for the asymmetric transfer hydrogenation of ketones to date. Recovery (~99%), reusability (fifth cycle, yield of 89% and ee of 81%), and stability of G-CLRu(II) were also found to be good. Overall, due to high activity, stability, reusability, and recovery, the preset stepwise preparation of G-CLRu(II) opens a new door for designing various chiral-centered heterogenized catalysts for asymmetric synthesis.

**Supplementary Materials:** The following are available online at <http://www.mdpi.com/2073-4344/10/2/175/s1>, Figure S1: HRTEM images of G-CLRu(II) and the corresponding SAED pattern and elemental mapping. Figure S2: XPS survey spectra of G-COOH, G-COCl, G-CONCS, G-Cl and G-CLRu(II). Figure S3: Deconvoluted XPS spectra of (a) C 1s and (b) O 1s peaks of G-COOH. Figure S4: Deconvoluted XPS spectrum of Cl 2p of G-COCl. Figure S5: Deconvoluted XPS spectrum of (a) N 1s and (b) S 2p of G-CONCS. Figure S6: Deconvoluted XPS spectrum of (a) N 1s and (b) S 2p of G-CL. Figure S7: HRTEM images of G-CLRu(II) after use. Figure S8: <sup>1</sup>H NMR spectra of G-CLRu(II). Figure S9: <sup>13</sup>C NMR spectra of G-CLRu(II). Figure S10: <sup>1</sup>H NMR spectra of G-COOH. Figure S11: <sup>13</sup>C NMR spectra of G-COOH. Figure S12: <sup>1</sup>H NMR spectra of G-CL. Figure S13: <sup>13</sup>C NMR spectra of G-CL. Figure S14: HPCL chromatogram of acetophenone. Figure S15: HPCL chromatogram of acetophenone after catalyzed by G-CLRu(II) under optimized reaction conditions.

**Author Contributions:** Conceptualization, methodology, original draft writing, review and editing, G.M., K.I.S. and C.I.M.; Formal analysis and supervision, G.M. and K.I.S.; Software and formal analysis, C.I.M. and G.M.; Data curation and investigation, C.I.M. and K.I.S. All authors have read and agreed to the published version of the manuscript.

**Funding:** This research received no external funding.

**Acknowledgments:** This study was supported by Konkuk University's KU research professor program.

**Conflicts of Interest:** The authors declare no conflict of interest.

## References

1. Li, Y.Y.; Yu, S.L.; Shen, W.Y.; Gao, J.X. Iron-, cobalt-, and nickel-catalyzed asymmetric transfer hydrogenation and asymmetric hydrogenation of ketones. *Acc. Chem. Res.* **2015**, *48*, 2587–2598. [[CrossRef](#)]
2. Zuo, W.; Lough, A.J.; Li, Y.F.; Morris, R.H. Amine (imine) diphosphine iron catalysts for asymmetric transfer hydrogenation of ketones and imines. *Science* **2013**, *342*, 1080–1083. [[CrossRef](#)]
3. Ikariya, T.; Blacker, A.J. Asymmetric transfer hydrogenation of ketones with bifunctional transition metal-based molecular catalysts. *Acc. Chem. Res.* **2007**, *40*, 1300–1308. [[CrossRef](#)] [[PubMed](#)]
4. Gladiali, S.; Alberico, E. Asymmetric transfer hydrogenation: Chiral ligands and applications. *Chem. Soc. Rev.* **2006**, *35*, 226–236. [[CrossRef](#)] [[PubMed](#)]
5. Han, Z.Y.; Xiao, H.; Chen, X.H.; Gong, L.Z. Consecutive intramolecular hydroamination/asymmetric transfer hydrogenation under relay catalysis of an achiral gold complex/chiral bronsted acid binary system. *J. Am. Chem. Soc.* **2009**, *131*, 9182–9183. [[CrossRef](#)] [[PubMed](#)]
6. He, Y.M.; Fan, Q.H. Phosphine-free chiral metal catalysts for highly effective asymmetric catalytic hydrogenation. *Org. Biomol. Chem.* **2010**, *8*, 2497–2504. [[CrossRef](#)] [[PubMed](#)]
7. Li, L.; Wu, J.; Wang, F.; Liao, J.; Zhang, H.; Lian, C.; Zhu, J.; Deng, J. Asymmetric transfer hydrogenation of ketones and imines with novel water-soluble chiral diamine as ligand in neat water. *Green Chem.* **2007**, *9*, 23–25. [[CrossRef](#)]
8. Baratta, W.; Da Ros, P.; Del Zotto, A.; Sechi, A.; Zangrando, E.; Rigo, P. Cyclometalated Ruthenium(II) Complexes as Highly Active Transfer Hydrogenation Catalysts. *Angew Chem. Int. Ed.* **2004**, *43*, 3584–3588. [[CrossRef](#)]
9. Sheeba, M.M.; Muthu Tamizh, M.; Farrugia, L.J.; Endo, A.; Karvembu, R. Chiral ( $\eta^6$ -p-Cymene)ruthenium(II) Complexes Containing Monodentate Acylthiourea Ligands for Efficient Asymmetric Transfer Hydrogenation of Ketones. *Organometallics* **2014**, *33*, 540–550. [[CrossRef](#)]
10. Collis, A.E.; Horvath, I.T. Heterogenization of homogeneous catalytic systems. *Catal. Sci. Technol.* **2011**, *1*, 912–919. [[CrossRef](#)]
11. Mihalcik, D.J.; Lin, W. Mesoporous silica nanosphere supported ruthenium catalysts for asymmetric hydrogenation. *Angew Chem. Int. Ed.* **2008**, *47*, 6229–6232. [[CrossRef](#)]
12. Sun, Y.; Liu, G.; Gu, H.; Huang, T.; Zhang, Y.; Li, H. Magnetically recoverable SiO<sub>2</sub>-coated Fe<sub>3</sub>O<sub>4</sub> nanoparticles: A new platform for asymmetric transfer hydrogenation of aromatic ketones in aqueous medium. *Chem. Commun.* **2011**, *47*, 2583–2585. [[CrossRef](#)] [[PubMed](#)]
13. Babin, M.; Clement, R.; Gagnon, J.; Fontaine, F.G. Homogeneous asymmetric transfer hydrogenation of ketones using a ruthenium catalyst anchored on chitosan: Natural chirality at work. *New J. Chem.* **2012**, *36*, 1548–1551. [[CrossRef](#)]
14. Tang, S.; Jin, R.; Zhang, H.; Yao, H.; Zhuang, J.; Liu, G.; Li, H. Recoverable organorhodium-functionalized polyhedral oligomeric silsesquioxane: A bifunctional heterogeneous catalyst for asymmetric transfer hydrogenation of aromatic ketones in aqueous medium. *Chem. Commun.* **2012**, *48*, 6286–6288. [[CrossRef](#)] [[PubMed](#)]
15. Sonnenberg, J.F.; Coombs, N.; Dube, P.A.; Morris, R.H. Iron nanoparticles catalyzing the asymmetric transfer hydrogenation of ketones. *J. Am. Chem. Soc.* **2012**, *134*, 5893–5899. [[CrossRef](#)] [[PubMed](#)]
16. Qiu, B.; Xing, M.; Zhang, J. Recent advances in three-dimensional graphene based materials for catalysis applications. *Chem. Soc. Rev.* **2018**, *47*, 2165–2216. [[CrossRef](#)]
17. Schaetz, A.; Zeltner, M.; Stark, W.J. Carbon modifications and surfaces for catalytic organic transformations. *ACS Catal.* **2012**, *2*, 1267–1284. [[CrossRef](#)]
18. Garrido-Barros, P.; Gimbert-Surinnach, C.; Moonshiram, D.; Picon, A.; Monge, P.; Batista, V.S.; Llobet, A. Electronic  $\pi$ -delocalization boosts catalytic water oxidation by Cu (II) molecular catalysts heterogenized on graphene sheets. *J. Am. Chem. Soc.* **2017**, *139*, 12907–12910. [[CrossRef](#)]
19. Kumar, S.; Khatri, O.P.; Cordier, S.; Boukherroub, R.; Jain, S.L. Graphene Oxide Supported Molybdenum Cluster: First Heterogenized Homogeneous Catalyst for the Synthesis of Dimethylcarbonate from CO<sub>2</sub> and Methanol. *Chem. Eur. J.* **2015**, *21*, 3488–3494. [[CrossRef](#)]
20. Zhao, Q.; Bai, C.; Zhang, W.; Li, Y.; Zhang, G.; Zhang, F.; Fan, X. Catalytic epoxidation of olefins with graphene oxide supported copper (Salen) complex. *Ind. Eng. Chem. Res.* **2014**, *53*, 4232–4238. [[CrossRef](#)]

21. Li, Z.; Wu, S.; Ding, H.; Zheng, D.; Hu, J.; Wang, X.; Huo, Q.; Guan, J.; Kan, Q. Immobilized Cu (II) and Co (II) salen complexes on graphene oxide and their catalytic activity for aerobic epoxidation of styrene. *New J. Chem.* **2013**, *37*, 1561–1568. [[CrossRef](#)]
22. Su, H.; Wu, S.; Li, Z.; Huo, Q.; Guan, J.; Kan, Q. Co (II), Fe (III) or VO (II) Schiff base metal complexes immobilized on graphene oxide for styrene epoxidation. *Appl. Organomet. Chem.* **2015**, *29*, 462–467. [[CrossRef](#)]
23. Shylesh, S.; Jia, M.; Thiel, W.R. Recent Progress in the Heterogenization of Complexes for Single-Site Epoxidation Catalysis. *Eur. J. Inorg. Chem.* **2010**, *2010*, 4395–4410. [[CrossRef](#)]
24. Kumar, S.; Kumar, P.; Deb, A.; Maiti, D.; Jain, S.L. Graphene oxide grafted with iridium complex as a superior heterogeneous catalyst for chemical fixation of carbon dioxide to dimethylformamide. *Carbon* **2016**, *100*, 632–640. [[CrossRef](#)]
25. Sabater, S.; Mata, J.A.; Peris, E. Catalyst enhancement and recyclability by immobilization of metal complexes onto graphene surface by noncovalent interactions. *ACS Catal.* **2014**, *4*, 2038–2047. [[CrossRef](#)]
26. Movahed, S.K.; Esmatpoursalmani, R.; Bazgir, A. N-Heterocyclic carbene palladium complex supported on ionic liquid-modified graphene oxide as an efficient and recyclable catalyst for Suzuki reaction. *RSC Adv.* **2014**, *4*, 14586–14591. [[CrossRef](#)]
27. Yang, Q.; Pan, X.; Clarke, K.; Li, K. Covalent functionalization of graphene with polysaccharides. *Ind. Eng. Chem. Res.* **2011**, *51*, 310–317. [[CrossRef](#)]
28. Sheeba, M.M.; Tamizh, M.M.; Bhuvanesh, N.S.; Karvembu, R. Water soluble Ru (II)-p-cymene complexes of chiral aroylthiourea ligands derived from unprotected D/L-alanine as proficient catalysts for asymmetric transfer hydrogenation of ketones. *Appl. Organomet. Chem.* **2019**, *33*, 4667. [[CrossRef](#)]
29. Mariconda, A.; Longo, P.; Agovino, A.; Guadagno, L.; Sorrentino, A.; Raimondo, M. Synthesis of ruthenium catalysts functionalized graphene oxide for self-healing applications. *Polymer* **2015**, *69*, 330–342. [[CrossRef](#)]
30. Fang, M.; Wang, K.; Lu, H.; Yang, Y.; Nutt, S. Covalent polymer functionalization of graphene nanosheets and mechanical properties of composites. *J. Mater. Chem.* **2009**, *19*, 7098–7105. [[CrossRef](#)]
31. Sheeba, M.M.; Preethi, S.; Nijamudheen, A.; Tamizh, M.M.; Datta, A.; Farrugia, L.J.; Karvembu, R. Half-sandwich Ru ( $\eta^6\text{-C}_6\text{H}_6$ ) complexes with chiral aroylthioureas for enhanced asymmetric transfer hydrogenation of ketones—experimental and theoretical studies. *Catal. Sci. Technol.* **2015**, *5*, 4790–4799. [[CrossRef](#)]
32. Deng, D.; Xiao, L.; Chung, I.M.; Kim, I.S.; Gopiraman, M. Industrial-quality graphene oxide switched highly efficient metal-and solvent-free synthesis of  $\beta$ -ketoenamines under feasible conditions. *ACS Sustain. Chem. Eng.* **2017**, *5*, 1253–1259. [[CrossRef](#)]
33. Zhou, X.; Zhang, T.; Abney, C.W.; Li, Z.; Lin, W. Graphene-Immobilized Monomeric Bipyridine- $\text{M}^{\text{x}+}$  ( $\text{M}^{\text{x}+} = \text{Fe}^{3+}, \text{Co}^{2+}, \text{Ni}^{2+}, \text{or } \text{Cu}^{2+}$ ) Complexes for Electrocatalytic Water Oxidation. *ACS Appl. Mater. Interfaces* **2014**, *6*, 18475–18479. [[CrossRef](#)] [[PubMed](#)]
34. Sheeba, M.M.; Tamizh, M.M.; Babu, S.G.; Bhuvanesh, N.S.; Karvembu, R. Ru (II)-p-cymene complexes containing esters of chiral D/L-phenylalanine derived aroylthiourea ligands for enantioselective reduction of pro-chiral ketones. *RSC Adv.* **2016**, *6*, 68494–68503. [[CrossRef](#)]
35. San Tan, S.; Yanagisawa, S.; Inagaki, K.; Kassim, M.B.; Morikawa, Y. Experimental and computational studies on ruthenium (ii) bis-diimine complexes of N, N'-chelate ligands: The origin of changes in absorption spectra upon oxidation and reduction. *Phys. Chem. Chem. Phys.* **2019**, *21*, 7973–7988. [[CrossRef](#)]
36. Ando, T.; Kamigaito, M.; Sawamoto, M. Catalytic activities of ruthenium (II) complexes in transition-metal-mediated living radical polymerization: Polymerization, model reaction, and cyclic voltammetry. *Macromolecules* **2000**, *33*, 5825–5829. [[CrossRef](#)]
37. Gopiraman, M.; Saravanamoorthy, S.; Deng, D.; Ilangovan, A.; Kim, I.S.; Chung, I.M. Facile Mechanochemical Synthesis of Nickel/Graphene Oxide Nanocomposites with Unique and Tunable Morphology: Applications in Heterogeneous Catalysis and Supercapacitors. *Catalysts* **2019**, *9*, 486. [[CrossRef](#)]
38. Gopiraman, M.; Ganesh Babu, S.; Khatri, Z.; Kai, W.; Kim, Y.A.; Endo, M.; Karvembu, R.; Kim, I.S. Dry synthesis of easily tunable nano ruthenium supported on graphene: Novel nanocatalysts for aerial oxidation of alcohols and transfer hydrogenation of ketones. *J. Phys. Chem. C* **2013**, *117*, 23582–23596. [[CrossRef](#)]
39. Zhang, S.; Zhang, F.; Pan, Y.; Jin, L.; Liu, B.; Mao, Y.; Huang, J. Multiwall-carbon-nanotube/cellulose composite fibers with enhanced mechanical and electrical properties by cellulose grafting. *RSC Adv.* **2018**, *8*, 5678–5684. [[CrossRef](#)]

40. You, X.; Zou, G.; Ye, Q.; Zhang, Q.; He, P. Ruthenium (II) complex-sensitized solid-state polymerization of diacetylene in the visible light region. *J. Mater. Chem.* **2008**, *18*, 4704–4711. [[CrossRef](#)]
41. Liu, Z.; Ou, J.; Wang, H.; You, X.; Ye, M. Synthesis and characterization of hydrazide-linked and amide-linked organic polymers. *ACS Appl. Mater. Interfaces* **2016**, *8*, 32060–32067. [[CrossRef](#)] [[PubMed](#)]
42. Chung, S.; Moon, J.M.; Choi, J.; Hwang, H.; Shim, Y.B. Magnetic force assisted electrochemical sensor for the detection of thrombin with aptamer-antibody sandwich formation. *Biosens. Bioelectron.* **2018**, *117*, 480–486. [[CrossRef](#)] [[PubMed](#)]
43. Varughese, B.; Chellamma, S.; Lieberman, M. XPS study of self-assembly of ruthenium dimers  $[(\text{acac})_2\text{Ru}(\text{2bptz})_0]^+$  on hydrophobic and hydrophilic SAMs. *Langmuir* **2002**, *18*, 7964–7970. [[CrossRef](#)]
44. Agnes, C.; Arnault, J.C.; Omnes, F.; Jousselme, B.; Billon, M.; Bidan, G.; Mailley, P. XPS study of ruthenium tris-bipyridine electrografted from diazonium salt derivative on microcrystalline boron doped diamond. *Phys. Chem. Chem. Phys.* **2009**, *11*, 11647–11654. [[CrossRef](#)]
45. Morgan, D.J. Resolving ruthenium: XPS studies of common ruthenium materials. *Surf. Interface Anal.* **2015**, *47*, 1072–1079. [[CrossRef](#)]
46. Gao, F.; Jin, R.; Zhang, D.; Liang, Q.; Ye, Q.; Liu, G. Flower-like mesoporous silica: A bifunctionalized catalyst for rhodium-catalyzed asymmetric transfer hydrogenation of aromatic ketones in aqueous medium. *Green Chem.* **2013**, *15*, 2208–2214. [[CrossRef](#)]
47. Li, J.; Zhang, Y.; Han, D.; Gao, Q.; Li, C. Asymmetric transfer hydrogenation using recoverable ruthenium catalyst immobilized into magnetic mesoporous silica. *J. Mol. Catal. A Chem.* **2009**, *298*, 31–35. [[CrossRef](#)]
48. Sandee, A.J.; Petra, D.G.; Reek, J.N.; Kamer, P.C.; van Leeuwen, P.W. Solid-phase synthesis of homogeneous ruthenium catalysts on silica for the continuous asymmetric transfer hydrogenation reaction. *Chem. Eur. J.* **2001**, *7*, 1202–1208. [[CrossRef](#)]
49. Jiang, H.Y.; Yang, C.F.; Li, C.; Fu, H.Y.; Chen, H.; Li, R.X.; Li, X.J. Heterogeneous Enantioselective Hydrogenation of Aromatic Ketones Catalyzed by Cinchona-and Phosphine-Modified Iridium Catalysts. *Angew Chem. Int. Ed.* **2008**, *47*, 9240–9244. [[CrossRef](#)]
50. Liu, P.N.; Gu, P.M.; Deng, J.G.; Tu, Y.Q.; Ma, Y.P. Synthesis of dendritic catalysts and application in asymmetric transfer hydrogenation. *Eur. J. Org. Chem.* **2005**, *2005*, 3221–3227. [[CrossRef](#)]
51. Liu, P.N.; Gu, P.M.; Wang, F.; Tu, Y.Q. Efficient heterogeneous asymmetric transfer hydrogenation of ketones using highly recyclable and accessible silica-immobilized Ru-TsDPEN catalysts. *Org. Lett.* **2004**, *6*, 169–172. [[CrossRef](#)] [[PubMed](#)]
52. Liu, P.N.; Deng, J.G.; Tu, Y.Q.; Wang, S.H. Highly efficient and recyclable heterogeneous asymmetric transfer hydrogenation of ketones in water. *Chem. Commun.* **2004**, *18*, 2070–2071. [[CrossRef](#)] [[PubMed](#)]
53. Liang, Y.; Jing, Q.; Li, X.; Shi, L.; Ding, K. Programmed assembly of two different ligands with metallic ions: Generation of self-supported Noyori-type catalysts for heterogeneous asymmetric hydrogenation of ketones. *J. Am. Chem. Soc.* **2005**, *127*, 7694–7695. [[CrossRef](#)] [[PubMed](#)]

